Single receiver Long-Term Evolution passive radar system using signal reconstruction for moving target detection

Lionel de Guenin, Patrick Rosson, Nicolas Petrochilos, Éric Moreau

Received: 4 June 2024 | Revised: 14 October 2024 | Accepted: 19 October 2024

IET Radar, Sonar & Navigation

DOI: 10.1049/rsn2.12662

The Institution of Engineering and Technology WILEY

ORIGINAL RESEARCH

Single receiver Long-Term Evolution passive radar system using signal reconstruction for moving target detection

Lionel de Guenin[1] | Patrick Rosson[1] | Nicolas Petrochilos[2] | Eric Moreau[3]

[1]CEA-Leti, Université Grenoble Alpes, Grenoble, France

[2]CReSTIC, University of Reims, Reims, France

[3]CNRS, LIS, University of Toulon, Toulon, France

Correspondence

Lionel de Guenin and Patrick Rosson.
Email: lionel.deguenin@gmx.fr and patrick.rosson@cea.fr

Abstract

This paper presents a single-antenna receiver passive radar system in the context of moving target detection such as trains, car, planes and UAVs, leveraging the long-term evolution (LTE) network as an illumination source. The proposed system uses signal reconstruction enabled by the telecom structure of the opportune signal in order to forego the use of a reference antenna. This presents the advantage of not relying on a physical signal for reference and its possible defect, potentially yielding better performances. The techniques introduced are validated through simulation and experiments. Moreover, a simplified passive radar system emphasises one of the key advantage of passive radar over other competing technologies for moving target detection: stealthiness and cost-effectiveness.

KEYWORDS

long term evolution, passive radar, radar detection

1 | INTRODUCTION

Passive radar systems are popular for detecting targets at range due to a number of advantages compared to its active counterparts. Their passive nature makes them stealthy, they can exploit opportunity signals and thus do not need allocated frequency bands, and are generally cost-effective both in terms of system and operating costs.

Digital video broadcasting-terrestrial (DVB-T)-based passive radar are effective to detect car/boat/aircraft/helicopter type targets at the deca-kilometre range [1–5]. They can fully exploit the relatively dense distribution of the DVB-T base stations (BS) and the orthogonal frequency division multiplexing (OFDM) nature of the signal. This presents numerous advantages for radar processes compared to other telecommunication wave-forms [1], such as faster cross correlation algorithms.

Nowadays affordable and easily accessible unmanned aerial vehicles as well as the prospect of autonomous vehicles presents new challenges for security of some sites. Sensible areas (as upcoming large-scale events, as well as scientific labs, factories etc.) could be perturbed by unwanted/unregulated vehicles. Previous works [6–8] have shown that cellular communications (4G/5G)-based passive radar can be adequate to detect such potential intruders. In ref. [9], a waveform analysis provides the possible/theoretical range and resolution of such detection systems, as well as possible ambiguities. Recently, in ref. [10] the authors proposed a 5G-based passive radar system for drone detection based on the same system architecture as that of DVB-T-based ones.

Classically, the passive radar system has one antenna dedicated to measuring a reference signal which is supposed to be clear of the moving target of interest. In this article, we propose to omit this extra antenna and attempt to reconstruct the emitted signal by using telecom processes: reading sufficient reference signals in order to reconstruct a part of the emitted signal. Then we use the said reconstructed signal to correct the received signal defaults: amplitude variations and time/frequency synchronisations offsets. Such signal reconstruction concept for passive radar has been studied for digital audio broadcasting [11], global system for mobile communications (GSM) [12], DVB-T [13–16] and Wi-Fi [17].

In contrast to other networks, 4G/5G long-term evolution (LTE) network offers a triple diversity [18]. Firstly, there is spatial diversity as the base station (BS) network is densely

populated with multiple stations per square kilometre, particularly in urban environments. Secondly, there's frequency diversity which spans LTE bands from 700 MHz to 2.6 GHz. Thirdly, there is polarization diversity with each BS emitting on multiple ports featuring orthogonal polarization.

By exploiting one or several of these diversities, we simplify the usual OFDM passive radar system architecture for moving target detection using signal reconstruction. In this article, 1) we present the design and its feasibility of a LTE passive radar without the need of a reference antenna; and 2) we demonstrate such a system with a real-world implementation.

This paper presents the use of a single receiver, multiple input single output LTE passive radar, in the context of target detection only. The use case considers a standard LTE scenario, which poses challenges for a single receiver configuration. While ref. [19] also proposes to forego the reference antenna thanks to signal reconstruction, they still use multiple reference antennas; moreover, they cannot afford to use OFDM radar processes in the frequency domain since they plan to detect targets (trains in this case) beyond the OFDM symbol range, and they do not present experimental results.

The remainder of the paper follows this structure: we begin by introducing the scenario and mathematical model, followed by a presentation of both classical and implemented radar processes. Subsequently, we compare simulation results with real measurements. Finally, we draw conclusions regarding the feasibility and performance of a simplified passive radar system.

2 | SCENARIO AND SIGNAL MODEL

The scenario studied in this paper is an elementary LTE scenario as displayed in Figure 1. The receiver is covered by several LTE Base Stations (BS), and has line of sight on the closest one, the position of which is known. This base station has up to 4 active ports of emission, their index is denoted by p and their emission signal by $x^p(t)$. Those signals propagates along three types of paths, the direct path d corresponds to the line of sight, the target path u corresponds to the reflection on the moving target and the multiple clutter paths c corresponds to the multiple reflections on diverse elements of the scene. Both the opportune emitter and the scene are static in respect to our receiver and the target is in motion, inducing a Doppler effect on the reflected signal along path u.

2.1 | Propagation

The general expression of the received signal, synchronised time-wise to the transmitter is given by the following equation:

$$y(t) = \sum_{p=1}^{P}\left[x^p\left(t-\tau_d^p\right)\alpha_d^p + \sum_{c=1}^{C} x^p\left(t-\tau_c^p\right)\alpha_c^p + \sum_{u=1}^{U} x^p\left(t-\tau_u^p\right)\beta_u^p e^{2i\pi\delta_u t}\right] + i(t) + b(t) \tag{1}$$

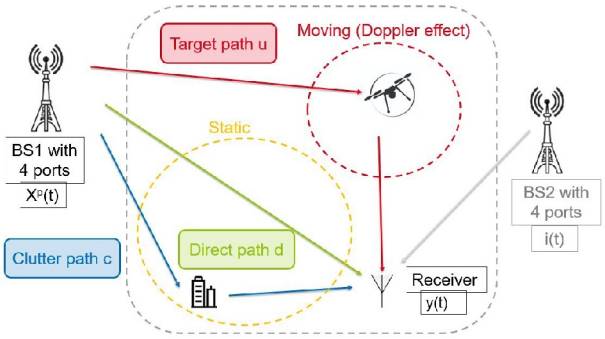

FIGURE 1 Long-term evolution (LTE) passive radar scenario.

with $x^p(t)$ the transmitted signal on port p, $y(t)$ the received signal; α_d^p, α_c^p, and β_u^p are coefficients corresponding to paths d, c, and u from port p; τ_c^p and τ_u^p are delays of paths c and u from port p; δ_u are Doppler shifts of paths u, $i(t)$ are inter-BS interferences, $b(t)$ is additive white gaussian noise (AWGN). For the sake of simplicity and given both the duration of signal acquisition and bandwidth of the signal, we assume that τ_u^p and β_u^p are constant for each of our procedure. The following expression can be summarised as a sum of contributions:

$$y(t) = y_{static}(t) + y_{target}(t) + i(t) + b(t) \tag{2}$$

where

$$y_{static}(t) = \sum_{p=1}^{P}\left[x^p\left(t-\tau_d^p\right)\alpha_d^p + \sum_{c=1}^{C} x^p\left(t-\tau_c^p\right)\alpha_c^p\right] \tag{3}$$

$$y_{target}(t) = \sum_{p=1}^{P}\left[\sum_{u=1}^{U} x^p\left(t-\tau_u^p\right)\beta_u^p e^{2i\pi\delta_u t}\right] \tag{4}$$

2.2 | Orthogonal Frequency Division Multiplexing waveform

The m^{th} OFDM symbol emitted from port p (4 ports maximum in LTE [18]) is written in the discrete temporal domain as $x^{m,p}[n]$; we then have the following equation:

$$x^{m,p}[n] = 0 \qquad n < mN \tag{5}$$

$$x^{m,p}[n] = \frac{1}{K}\sum_{k=-\frac{K}{2}}^{\frac{K}{2}-1} X^{m,p}[k]e^{2i\pi\frac{k}{K}(n-N_{CP}-mN)} \qquad mN \le n < ((m+1)N) \tag{6}$$

$$x^{m,p}[n] = 0 \qquad ((m+1)N) \le n \tag{7}$$

with $X^{m,p}[k]$ the m^{th} quadrature amplitude modulation symbol of sub-carrier k transmitted from port p, $0 < n < NM$ the

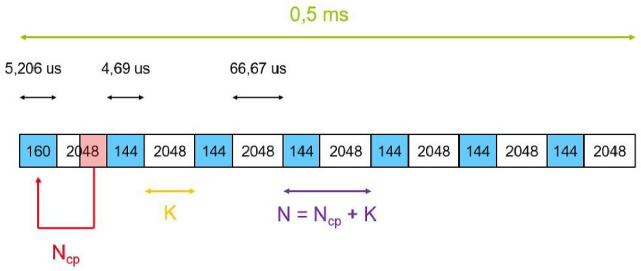

FIGURE 2 Long-term evolution (LTE) orthogonal frequency division Multiplexing (OFDM) slot structure for 20 MHz.

global discrete temporal variable at the transmitter, sampled at T_s time intervals, M the total number of OFDM symbol, N the OFDM symbol length, K the total number of sub-carrier (i.e. the size of the inverse discrete Fourier transform), and N_{CP} the length of the Cyclic Prefix (CP).

$$N = N_{CP} + K \tag{8}$$

Figure 2 represents a sequence of 7 OFDM symbols, called a slot, for a 20 MHz band in LTE [18].

A sequence of M OFDM symbol transmitted from port p in base-band is given by the following equation:

$$x_{bb}^{p}[n] = \sum_{m=0}^{M-1} x^{m,p}[n] \tag{9}$$

Transmitted signal post analogue/digital conversion, filtering and high-frequency conversion to central frequency f_{TX}:

$$x^{p}[n] = \Re\left(x_{bb}^{p}[n]e^{2i\pi f_{TX}n}\right) \tag{10}$$

We extract $x_{cpless}^{p}[n]$ the sequence without CP, (forced to 0) from $x^{p}[n]$:

$$x_{cpless}^{p}[n] = \sum_{m=0}^{M-1} x_{cpless}^{m,p}[n] \tag{11}$$

with the emitted CP-less OFDM symbols m on port p:

$$x_{cpless}^{m,p}[n] = 0 \quad n \notin [(m-1)N + N_{CP}, mN[\tag{12}$$

$$x_{cpless}^{m,p}[n] = x^{m,p}[n] \quad n \in [(m-1)N + N_{CP}, mN[\tag{13}$$

2.3 | Long-Term Evolution reference and synchronisation signals

The emitted signal follows the LTE norm [18], as certain part of the signal is composed of control signals with particular properties. There is two types of control signals that are of particular interest for our purposes, the Cell-specific Reference Signals (C-RS) and the two synchronisation signals: the Primary Synchronisation Sequence (P-SS) and Secondary Synchronisation Sequence (S-SS). The physical broadcast channel, physical downlink control channel, and physical downlink shared channel are control and data signals which are dependent on the traffic state. A general overview of the time–frequency structure of the LTE signal is recapitulated in Figure 3 (provided from ref. [23]).

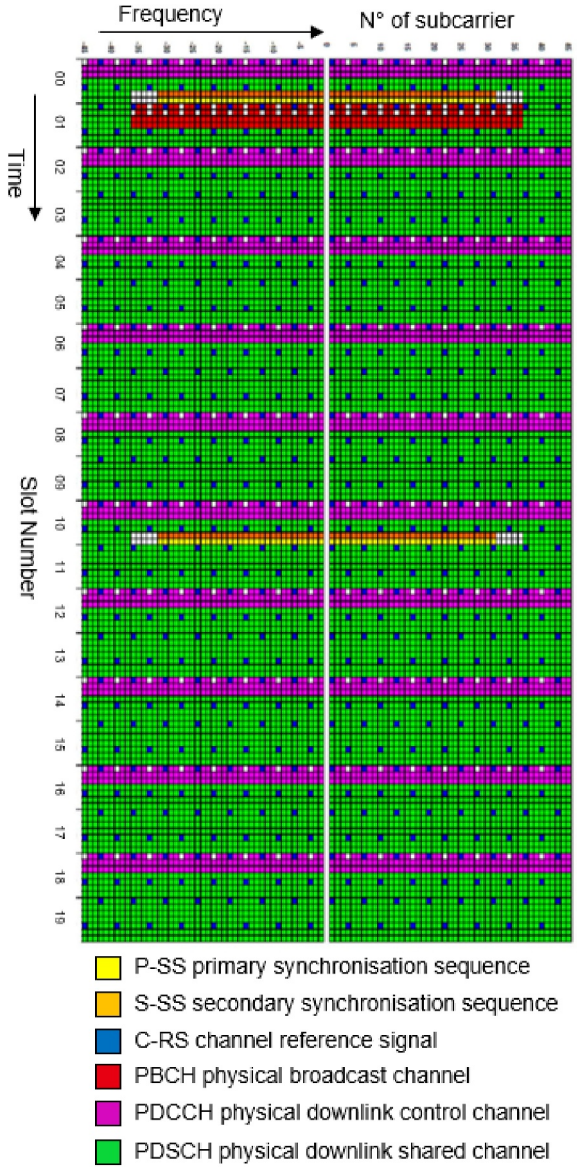

FIGURE 3 Long-term evolution (LTE) frame time/frequency structure for the central 1.4 MHz band.

Primary Synchronisation Sequence and S-SS are known sequences which provide the identity of the BS, and allows for the reconstruction of the complete C-RS series.

Using the known C-RS, we introduce the masked signals $Y^{m,p}[\kappa]$ and $\tilde{X}^{m,p}[\kappa]$, received and estimated, respectively (in the frequency domain). With κ, the set the indexes of the

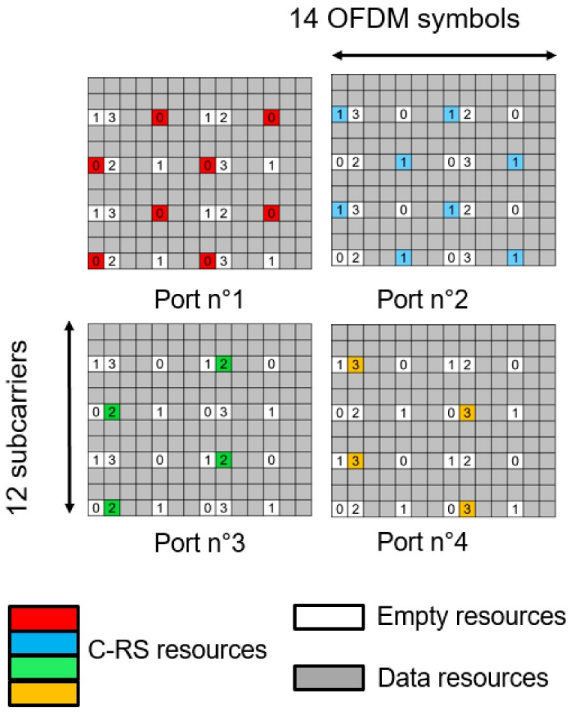

FIGURE 4 Cell-specific Reference Signals (C-RS) time/frequency structure.

sub-carriers hold a C-RS for an OFDM symbol m on port p. Since the active sub-carriers holding C-RS for a given port p vary with OFDM symbol m, for the sake of simplicity κ will also be used as the discreet frequency variable denoting an active sub-carrier holding a C-RS, although it also depends on p and m. The C-RS are distributed evenly in the time/frequency domain in a checkerboard-like pattern, where each emission port have its own dedicated C-RS pattern, which is displayed in Figure 4. The C-RS properties are as such:

- C-RS are exclusive:

$$\forall \kappa, \exists p_\kappa, \forall p' \neq p_\kappa, X^{m,p'}[\kappa] = 0 \tag{14}$$

We note p_κ the active port for κ.

- C-RS are always active:

$$X^{m,p_\kappa}[\kappa] \neq 0 \tag{15}$$

- C-RS are perfectly known:

$$\tilde{X}^{m,p_\kappa}[\kappa] = X^{m,p_\kappa}[\kappa] \tag{16}$$

Figure 4 (from ref. {22}) illustrates the temporal and frequency allocation pattern of C-RS for each port.

2.4 | Received signal

The discrete time propagation equation, with the received signal synchronised to a direct path of delay $\tau_d^{p_d}$ transmitted by port $p = p_d$.

$$\begin{aligned} y[n'] = &\sum_{p=1}^{P} \left[x^p\left[n' - \tau_d^p + \tau_d^{p_d}\right]\alpha_d^p\right. \\ &+ \sum_{c=1}^{C} x^p\left[n' - \tau_c^p + \tau_d^{p_d}\right]\alpha_c^p \\ &\left.+ \sum_{u=1}^{U} x^p\left[n' - \tau_u^p + \tau_d^{p_d}\right]\beta_u^p e^{2i\pi\delta_u n'}\right] \\ &\times e^{\left(-2i\pi f_{CFO} n'\right)} + b[n'] \end{aligned} \tag{17}$$

with $0 < n' < NM$ the global discrete temporal variable at the receiver, sampled at T_s' time intervals. In discrete time, $\tau_d^{p_d}$ is not an exact multiple of time resolution of the receiver $T_s' = \frac{T_K}{K}$, with T_K the CP-less OFDM symbol duration. This time offset is noted as follows:

$$\tau_{offset}^p = \tau_d^{p_d} \bmod T_s' = \tau_d^{p_d} \bmod \frac{T_K}{K} \tag{18}$$

Furthermore, the received signal is not down-converted to base-band with the same frequency to which the emitted signal was up-converted from base-band:

$$y_{bb}[n'] = y[n']e^{-2i\pi f_{RX} n'} \tag{19}$$

with the carrier frequency offset (CFO) with corresponding frequency difference f_{CFO} being:

$$e^{\left(2i\pi f_{TX} n\right)} e^{\left(-2i\pi f_{RX} n\right)} = e^{\left(-2i\pi f_{CFO} n\right)} \tag{20}$$

Moreover, the sampling frequency at the receiver is again expectedly different than the emitted one:

$$T_s' = T_s + \delta_t \tag{21}$$

with δ_t the sampling frequency offset (SFO) and T_s the sampling duration at the transmitter.

Thanks to time-synchronisation allowed by the CP, we can segment y into OFDM symbols:

$$y[n'] = \sum_{m=0}^{M-1} y^m[n'] \tag{22}$$

We build $y_{cpless}[n']$, the CP-less received signal:

$$y_{cpless}[n'] = \sum_{m=0}^{M-1} y_{cpless}^m[n'] \tag{23}$$

$$y^m_{cpless}[n'] = y^m[n'] \qquad n' \in [(m-1)N + N_{CP}, mN[\quad (24)$$

$$y^m_{cpless}[n'] = 0 \qquad n' \notin [(m-1)N + N_{CP}, mN[\quad (25)$$

and build $Y^m[k]$, the received signal in the frequency domain:

$$Y^m[k] = \frac{1}{K} \sum_{n'=mN+N_{CP}}^{(m+1)N} y^m_{cpless}[n'].e^{-2i\pi\frac{k}{K}(n'-N_{CP}-mN)} \quad (26)$$

Assuming that the maximum delay of the physical propagation channel is inferior to the CP length, $\max(\tau_c^p) < N_{CP}$, we can express the received signal in the frequency domain as a product of three terms. Those terms are the emitted signal $X^{m,p}[k]$, the physical propagation channel in the frequency domain $H^p_\mu[k]$, and an asynchronous factor $\Psi^{m,p}[k]$ that gather the different linear effects of CFO, SFO and time offset. An additive term $ICI^{m,p}[k]$ gathers the non-linear effects of CFO and SFO called inter carrier interference (ICI). According to refs. [20, 21], ICI is akin to additive noise and is usually small compared to thermal noise $B[k]$, thus it will be incorporated into the additive noise term $B'[k]$ with the AWGN:

$$Y^m[k] = \sum_{p=1}^{P} \Psi^{m,p}[k] H^p_\mu[k] X^{m,p}[k] + ICI^{m,p}[k] + B[k] \quad (27)$$

$$Y^m[k] = \sum_{p=1}^{P} \Psi^{m,p}[k] H^p_\mu[k] X^{m,p}[k] + B'[k] \quad (28)$$

where the measured frequency propagation channel $H^p_\mu[k]$ is the discrete Fourier transform of the physical propagation channel $h^p(\tau)$, with τ the continuous delay variable. $h^p(\tau)$ is the time channel impulse response of the propagation coefficients in Equation (1), and ηT_s (with $\eta \in \mathbb{Z}$) is a discrete local delay variable.

$$H^p_\mu[k] = \frac{1}{K} \sum_{\eta=0}^{K-1} h^p[\eta T_s] e^{-2i\pi\frac{k}{K}[\eta T_s]} \quad (29)$$

Tthe linear receiver imperfections effects $\Psi^{m,p}[k]$ are expressed as follows:

$$\Psi^{m,p}[k] = e^{2i\pi\left[f_{CFO}\frac{T_K}{K} + \frac{kT_K}{K\tau^p_{offset}} + \left(\frac{T'_s - T_s}{T_s}\right)k\left(\frac{mN+N_{cp}}{K}\right)\right]} \times sinc\left(\pi\left(f_{CFO}NT_s + \frac{T'_s - T_s}{T_s}k\right)\right) \quad (30)$$

3 | DETECTION PROCESS

3.1 | Classical approach

In the classical OFDM passive radar scenario, the reference signal is $x[n]$ measured and the transmitter of opportunity only has one transmission port $P = 1$, the inter base station interferences are usually negligible $i(t) = 0$.

3.1.1 | Cross Ambiguity Function and delay-Doppler plane

The response of each path in the received signal is calculated as a matched filter between the received signal and a Doppler shifted version of the reference signal called Cross Ambiguity Function (CAF). The CAF associates an energy amount to each potential path characterised by a delay and a Doppler-shift. It has been shown that this process can be calculated much faster in the frequency domain, without much loses in performance (see [24]). The response of a potential target in the delay-Doppler plane is described thanks to the AF, the impulse response of the cross-ambiguity process. The general expression of the ambiguity function $AF(\tau, \nu)$ of a continuous signal $x(t)$ is expressed as the square of the principal term $\chi(\tau, \nu)$:

$$AF(\tau, \nu) = |\chi(\tau, \nu)|^2 \quad (31)$$

with:

$$\chi(\tau, \nu) = \int_{-\infty}^{\infty} x(t)x(t-\tau)^* e^{-2i\pi\nu t} dt \quad (32)$$

Then the discrete time-limited AF of a real signal $x[n]$ composed of N samples can be defined as follows:

$$AF_K(n_\tau, \nu) = \left|\chi_{xx}(n_\tau, \nu)\right|^2 \quad (33)$$

$$\chi_{xx}(n_\tau, \nu) = \sum_{n=0}^{N} x[n]x[n-n_\tau]^* e^{-2i\pi\nu n} \quad (34)$$

Thus the CAF of a surveillance signal $y[n]$ with a reference signal $x[n]$ is calculated as follows:

$$CAF(n_\tau, \nu) = \left|\chi_{xy}(n_\tau, \nu)\right|^2 \quad (35)$$

$$\chi_{xy}(n_\tau, \nu) = \sum_{n=0}^{N} y[n]x[n-n_\tau]^* e^{-2i\pi\nu n_\tau} \quad (36)$$

For OFDM signals, it can be shown that the CAF can be calculated in the frequency domain under certain conditions (see [2]). Those conditions are that the considered delays must

be inferior to the OFDM symbol length and that the time spread of the propagation channel is inferior to the length of the CP. We then have, for a single reference signal:

$$\chi_{xy}[n_\tau,\nu]=\sum_{m=0}^{M-1}e^{(-2i\pi\nu mN)}\sum_{k=1}^{N}Y^m[k]X^m[k]^*e^{2i\pi\frac{k}{K}n_\tau} \quad (37)$$

where $Y^m[k]$ and $X^m[k]$ are the complex values of the k^{th} sub-carrier of the m^{th} OFDM symbol in the frequency domain of the surveillance signal and reference signal, respectively. Analysis of the AF of the C-RS LTE signal is discussed in-depth in ref. [9], and the results indicate that the level of the "floor" of the cross-ambiguity function of LTE pilots is too high to detect low radar cross section (RCS) targets. In other words, the coherence between the direct signal and a delayed, Doppler-shifted version of itself is too high. The level of this so called OFDM-floor level is provided by the following equation [2]:

$$\begin{aligned}&\mathrm{Var}\left\{\left|\chi_{xy}(\tau,\nu)\right|^2\right\}\simeq\frac{\left(|\alpha_d|+\sum_{c=1}^{C}|\alpha_c|\right)^2}{M}\mathrm{Var}\{AF_K\}\\&\mathrm{Var}\{AF_K\}=\frac{1}{K}\left(\mathbf{E}(|X^m[k]|)^4-1\right)\end{aligned} \quad (38)$$

with $\left|\chi_{xy}(\tau,\nu)\right|^2$ cross-ambiguity function of emitted signal x with received y, AF_K the discrete time-limited AF of received signal x, and $\mathbf{E}$ the expected value operator.

3.1.2 | Classic Orthogonal Frequency Division Multiplexing passive radar process

In order to remove those contributions in the cross-ambiguity function, clutter removal has to be performed. This process removes the contributions of the zero-Doppler paths in the received signal in order to remove their effect in the delay-Doppler space of the CAF. In essence, clutter removal is a channel estimation of the zero Doppler paths, due to the OFDM nature of the signal such channel estimation and the subsequent subtraction can be done in the frequency domain under certain constraints and hypothesis. Namely, the time spread of the channel has to be inferior to the CP length (see [1, 2]) and considered delays can only be inferior to the OFDM symbol duration. Those are the same that limit the calculation of the CAF in the frequency domain. Additionally, the perceived propagation channel must be time-invariant, which is practically true in most cases. This is because, for the measurement duration, all the effects of time-offsets, CFO and SFO can be reasonably assumed to be the same for both the reference and the surveillance signal, as they are measured with the same system.

Nonetheless, those OFDM-based frequency domain methods yield very similar results as their time domain counterparts for faster calculations. [24, 25] describe a method for OFDM based signal clutter cancelation that goes as follows:

For each sub-carrier k, a noise subspace vector, $\mathbf{C_{X,k}}$ is built on M symbols and is of M,1 dimension:

$$\mathbf{C_{X,k}}=\left[C_{X,k}[1],\ldots,C_{X,k}[m],\ldots,C_{X,k}[M]\right]^T \quad (39)$$

$$C_{X,k}[m]=\tilde{X^m}[k] \quad (40)$$

with $\tilde{X^m}[k]$ the estimated complex value of the reference signal for sub-carrier k and OFDM symbol m. ECA-C [24] uses this projection as is, but following ECA-CD [25] implies an extension to low Doppler shifts. Those low Doppler shifts are chosen to be smaller than what is expected to be detected, their frequency is noted f_{ECA-CD}.

$$\mathbf{C_{X,k}^{ECA-CD}}=\left[\Lambda^*\mathbf{C_{X,k}}|\mathbf{C_{X,k}}|\Lambda\mathbf{C_{X,k}}\right] \quad (41)$$

with $\mathbf{C_{X,k}^{ECA-CD}}$ a $M\times 3$ matrix and Λ a $M\times M$ diagonal matrix whose diagonal λ is:

$$\lambda=\left[1\quad e^{j2\pi f_{ECA-CD}T_s}\quad\ldots\quad e^{j2\pi f_{ECA-CD}MT_s}\right] \quad (42)$$

with T_s the duration of the OFDM symbol.

The projection matrix on clutter subspace M,M matrix P_k for the k^{th} sub-carrier is then calculated as follows:

$$\mathbf{P_k}=\mathbf{C_{X,k}}\left(\mathbf{C_{X,k}}^H\mathbf{C_{X,k}}\right)^{-1}\mathbf{C_{X,k}}^H \quad (43)$$

or

$$\mathbf{P_k}=\mathbf{C_{X,k}^{ECA-CD}}\left(\mathbf{C_{X,k}^{ECA-CD}}^H\mathbf{C_{X,k}^{ECA-CD}}\right)^{-1}\mathbf{C_{X,k}^{ECA-CD}}^H \quad (44)$$

Finally, the projection on the orthogonal subspace to the clutter:

$$\mathbf{P'_k}=(\mathbf{I}-\mathbf{P_k}) \quad (45)$$

The CAF is then calculated in the frequency domain as is discussed in Section 3.1.1. Figure 5 presents a typical system architecture for an OFDM passive radar system.

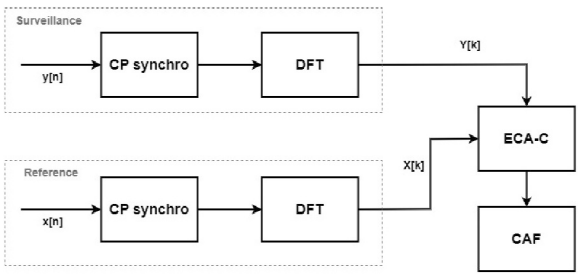

FIGURE 5 Bloc diagram of a typical orthogonal frequency division multiplexing (OFDM) passive system.

3.2 | Novel approach with signal reconstruction

Our use case requires us the exploitation of multiple reference signals, which differ from the classical case, given that the channel is different for each port, up to four distinct radar processes have to be made before a recombination.

Furthermore the classic OFDM clutter removal process relies on the time-invariant channel hypothesis; however, in our use case, the received signal is affected by both imperfections of the receiver and possible interference while the reference signal is not; ref. [17] illustrates this issue in their Wi-Fi passive radar scenario. Thus channel coefficients vary over time (see Figures 6 and 7 for example), invalidating this hypothesis. The aforementioned effects have first to be corrected: by telecom processes correcting the phase variations of the received signal and then by implementing an adjustment to clutter removal that takes into account varying amplitude of the received signal. It can be noticed that reference [15, 16], with their aeroported DVB-T-based passive radar is confronted with a similar problem, where their perceived channel is affected by a 2-D phase ramp in the temporal domain due to a moving receiver, causing Doppler effect and varying time-offsets symbol to symbol. They correct those in the time domain using a demod/remod approach. On the other hand, our signal is affected by CFO, SFO and a constant time offset, resulting in a perceived channel that is affected by a 2-D phase ramp in the frequency domain. As such our processes do not have to contend with switching back to the temporal domain, making them more streamlined and less computationally intense.

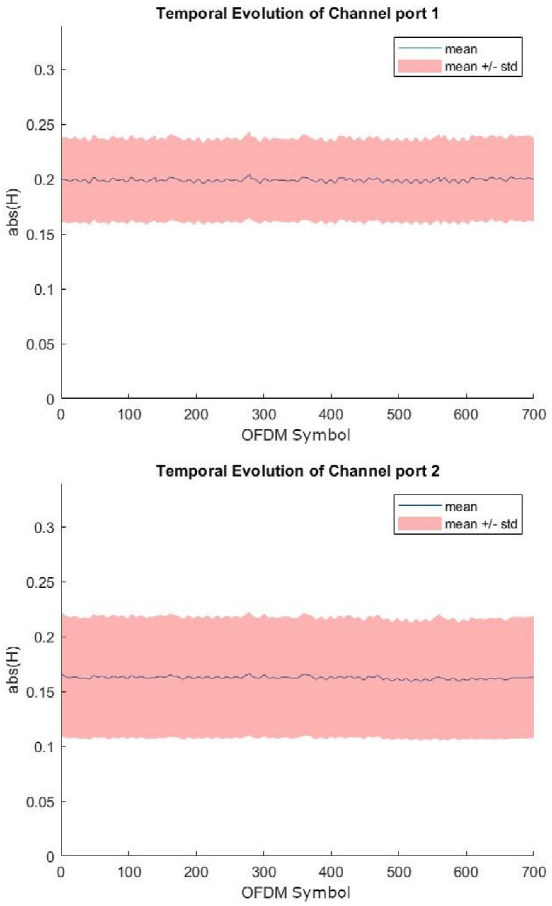

FIGURE 6 Temporal variations of the first two order statistics of the estimated channels for detection of plane.

3.2.1 | Telecom process

Coarse time and frequency synchronisation of the received signal are realised using the CP. This allows the construction of the received OFDM signal in the frequency domain from the CP-less received temporal signal: $Y^{m,p}[\kappa]$. Using the known P-SS and S-SS signals, we reconstruct our reference signal $X^{m,p}[\kappa]$. Note that contrary to a measured reference signal, our reconstructed signal is predetermined; thus, it is neither noisy nor affected by a secondary multipath channel. A preliminary channel estimation is done via zero-forcing on the C-RS of each frame. This estimated Zero Forced (ZF) channel is noted $H^{m,p}_{ZF0}[k]$ and is interpolated by the following equation:

$$H^{m,p}_{ZF0}[\kappa] = \frac{Y^{m,p}[\kappa]}{X^{m,p}[\kappa]} \tag{46}$$

While $Y^{m,p}[\kappa]$ is affected by imperfections at the receiver, that is time-offset, CFO and SFO; $X^{m,p}[\kappa]$ is not, and the time-invariant channel condition isn't verified for $H^{m,p}_{ZF0}[\kappa]$. Thus why a finer time and frequency synchronisation is done on this first channel estimation. Time and frequency offset in the frequency domain manifest themselves as a phase ramp and phase offset of the signal respectively. Two simple linear interpolations of the phase of this first channel estimation is done frame by frame, then subcarrier by subcarrier. The resulting estimated 2-D phase ramp is subsequently subtracted from both the received signal and the ZF channel.

$$H^{m,p}_{ZF0}[k] = H^{m,p}_{ZF}[k] e^{2i\pi\left[f_{CFO}\frac{T_K}{K} + \frac{kT_K}{K\tau^p_{offset}} + \left(\frac{T'_s - T_s}{T_s}\right)k\left(\frac{mN + N_{cp}}{K}\right)\right]} \tag{47}$$

3.2.2 | Implemented Long-Term Evolution radar process

The telecom process only corrects the phase of the received signal and estimated channel. The possible amplitude variations due to CFO (see Equation (30)) and eventual interference are still present in the signal. To remedy this, we propose to adjust the estimated channel coefficient for each OFDM symbol by a factor $\mu^p[m]$: the mean of the absolute value of the channel coefficients over the m^{th} OFDM symbol divided by the mean of the mean of the absolute values of the channel coefficients:

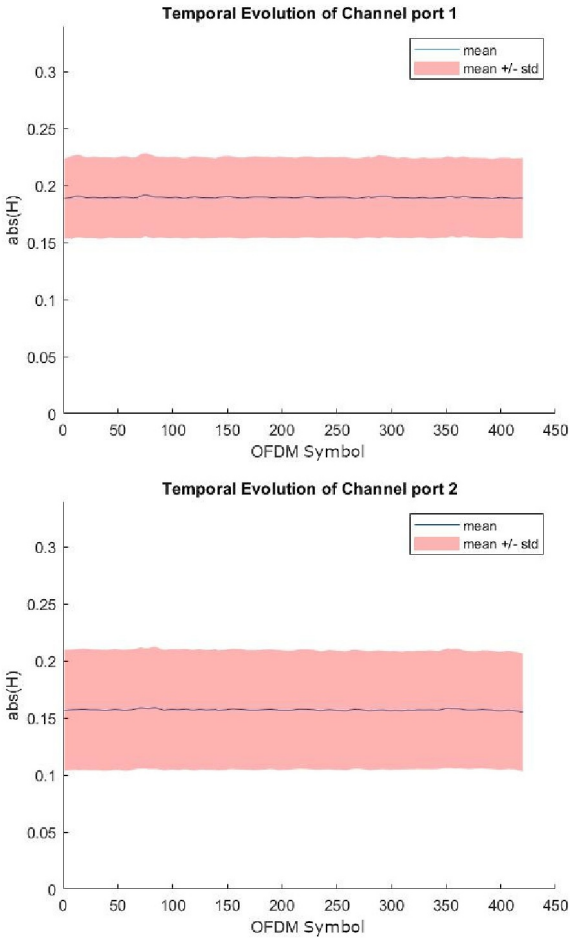

FIGURE 7 Temporal variations of the first two order statistics of the estimated channels for detection of car.

$$\mu^p[m] = \frac{\frac{1}{K}\sum_{k=1}^{K}|H_{ZF0}^{m,p}[k]|}{\frac{1}{KM}\sum_{m=1}^{M}\sum_{k=1}^{K}|H_{ZF0}^{m,p}[k]|} \tag{48}$$

The implemented clutter cancelation is done over each C-RS series emitted by each ports. For each sub-carrier k, a noise subspace vector $\mathbf{C}^{\mathbf{p}}_{\mathbf{X},\mathbf{k}}$ is built on M symbols:

$$\mathbf{C}^{\mathbf{p}}_{\mathbf{X},\mathbf{k}} = \left[C^p_{X,k}[1], \ldots, C^p_{X,k}[m], \ldots, C^p_{X,k}[M]\right]^T \tag{49}$$

$$For \quad k = \kappa(m,p) \quad : \quad C^p_{X,k}[m] = \widetilde{X^{m,p}}[\kappa(m,p)] \tag{50}$$

with $\widetilde{X^{m,p}}[\kappa]$ the estimated complex value of the reference signal for port p, sub-carrier k and OFDM symbol m.

$$H_\kappa^{p,clutter}[k] = \left(\mathbf{C}^{\mathbf{p}}_{\mathbf{X},\mathbf{k}}{}^H \mathbf{C}^{\mathbf{p}}_{\mathbf{X},\mathbf{k}}\right)^{-1} \mathbf{C}^{\mathbf{p}}_{\mathbf{X},\mathbf{k}}{}^H Y[\kappa(m,p)]$$
$$for \quad k \neq \kappa(m,p) \quad : \quad C^p_{X,k}[m] = 0 \quad and \quad H_\kappa^{p,clutter}[k] = 0$$
$$because \quad Y[k \neq \kappa(m,p)] = 0 \tag{51}$$

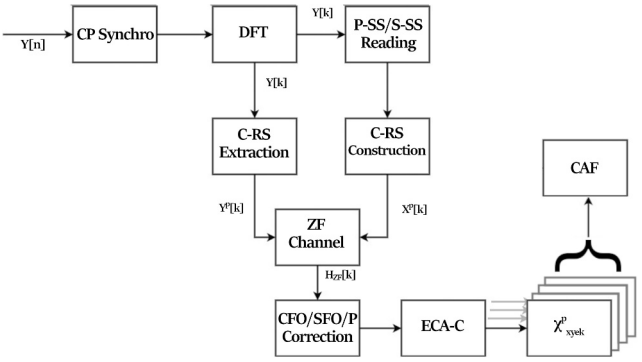

FIGURE 8 Bloc diagram of the proposed system.

Then the estimated clutter coefficient are adjusted by factor $\mu^p[m]$.

$$\tilde{Y}^{m,p}_{clutter,\varkappa}[k] = \mu^p[m] H_\kappa^{p,clutter}[k] X^p[\kappa(m,p)] \tag{52}$$

Finally, the principal term of the CAF for port p is calculated as such, note that we choose to normalise with respect to useful signal duration MK:

$$\chi^p_{xyex}[n_\tau, \nu] = \frac{1}{MK}\sum_{m=0}^{M-1} e^{(-2i\pi\nu mN)}$$
$$\sum_{k=1}^{N}\left[\left(Y^{m,p}(\kappa(m,p)) - \tilde{Y}^{m,p}_{clutter,\varkappa}(k)\right)X^{m,p}(\kappa(m,p))^*\right]e^{2i\pi\frac{k}{K}n_\tau} \tag{53}$$

The phase of the principal term $\chi^p_{xyex}(n_{\tau_u}, \nu_u)$ evaluated at the coordinates (n_{τ_u}, ν_u) of a potential target doesn't vary much with the emission port. We can thus combine the P principal terms by adding them before taking their absolute value. This approach coherently sums the potential response from targets and reduces the overall noise level.

$$CAF_{xyex}(n_\tau, \nu) = \left|\left|\sum_{p=0}^{P}\chi^p_{xyex}(n_\tau, \nu)\right|\right|^2 \tag{54}$$

Figure 8 summarises the proposed system architecture presented in this section.

4 | RESULTS

In this section, application of the discussed single receiver processes in a real scenario will be shown, as well as simulations results of the scenario for comparison, both for a standard system and for a single receiver system. First a detailed description of the measurement campaign with its geometry and a preliminary power budget will be shown with the results of detecting a car using our novel approach. Secondly a plane's

detection will be presented. For each case, results of two types of simulation will also be shown for comparison, one simulating the performance of our signal reconstruction based process and one replicating the performance of a standard multi-receiver in an equivalent ideal case.

4.1 | Car detection scenario

The measurement campaign was done at Gières, France, (45 ° 11′09.6”N, 5 ° 47′36.8”E) next to a road and a railway track for target variety, with multiple base stations in-range. The receiver had clear line of sight with respect to both the base station and the potential targets.

Figure 9 shows the geometry of the experiment: the red star denotes the position of the receiver, the red triangle the LTE BS and the green ellipse the area where targets have been acquired. Multiple types of targets are available in this configuration: trains and cars moving along the road/tracks but also small propeller-driven aircraft flying overhead, following a trajectory that is approximately parallel to those tracks/road, headed to landing in a near airfield at Gières. Table 1 shows the characteristic of the BS.

The passive radar is a directive antenna Siretta (data-sheet: [26]) connected to a ZNL 14 IQ analyser with a sampling frequency $F_s = 30.72$ MHz, which allows complete observation (20 MHz bandwidth, $K = 2048$) of the 2680 MHz LTE band operated by FREE, and used exclusively by the station. Acquisition has been done with azimut 105° (targeting the green ellipse on Figure 9), for a total acquisition time of 400 ms. The overhaul power budget of this campaign is shown in Figure 10 and Table 2, where out of band noise is about 30 dB below signal level.

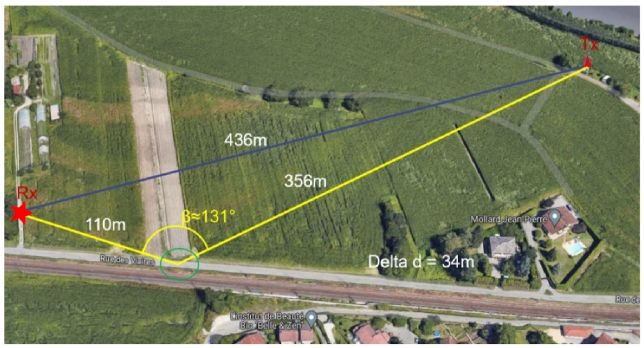

FIGURE 9 Top view of the acquisition site.

TABLE 1 Characteristics of the base station.

Operator FREE
Azimuts: 60°,240°,340°
Antenna height: 17.8 m
Frequency bands in MHz: 2600, 2100, 1800, 700 MHz

For a car target, only 3 frames (30 ms, $M = 420$) of acquisition are processed. Post coarse time/frequency synchronisation, the P-SS and S-SS allocated resources (see Figure 3) are extracted and decoded. This allows the deduction of the Cell ID of the base station (in this case cell ID 1 of 33 and cell ID 2 of 1, for a Physical Cell ID of 100), and the construction of the complete C-RS series, generating the two reference signals. Cell-specific Reference Signals extraction is done on the received signal, creating the two surveillance signals, using the two reference signals, the ZF-channel estimation is then done on each of those pair of signals. Carrier frequency offset and SFO compensation is done via a 2-D linear regression of the phase of the preliminary ZF-channel, to adjust both the received signal and the ZF-channel. This allows evaluation of the temporal variation of the channel power on this new corrected ZF-channel. Figure 7 shows those variations over the duration of the acquisition, for port 1 and 2 respectively. In this case the variation of the mean are very small but exhibits a “seesaw” pattern. We observe that the power allocated to C-RS varies across different symbols within the same slot (see Figure 4). Moreover the overall received power of each port is different, confirming the need to process those independently.

The two clutter cancellations are then done using the channel adjustment temporal factor, in order to subsequently calculate the two CAFs and their combination. Both 2D and 3D representation of the final CAFs measured are shown in

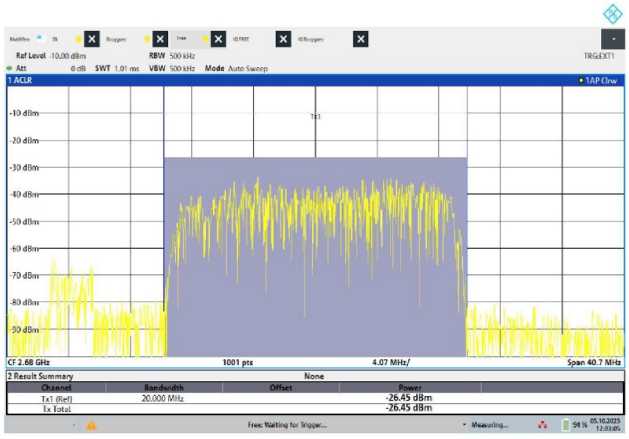

FIGURE 10 Power spectrum of the acquisition.

TABLE 2 Power budget of the acquisition.

Tx power	50 dBm
Tx antenna gain	17.5 dBi
Frequency	2.680 GHz
Bandwidth	20 MHz
Rx-Tx spacing	436 m
Rx antenna gain	5 dBi
Rx received power	−21 dBm

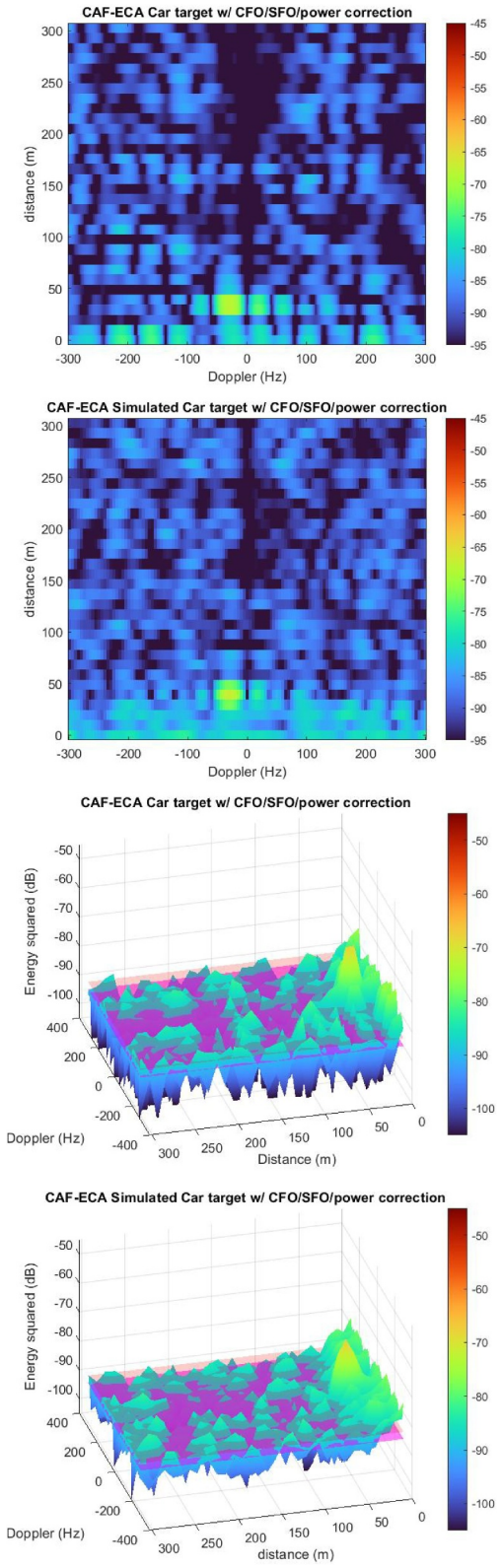

FIGURE 11 2D and 3D representation of the cross ambiguity function (CAF) post adjusted ECA-C, for a car target, using both real measurement (first and third) and simulation (second and fourth).

Figure 11. As a point of comparison results from simulation will also be shown. The Tx parameters, Rx parameters and geometry used for the simulation are those described above.

TABLE 3 Car target: Power levels in the delay-Doppler plane for adjusted ECA-C.

Adjusted ECA-C	Real	Simulations
Target response	−68.12 dB	−67.11 dB
Floor mean level	−90.09 dB	−89.34 dB
Floor mean + std level	−87.39 dB	−86.88 dB
Wall mean level	−82.79 dB	−81.55 dB
Target - (Floor mean + std level)	19.27 dB	19.77 dB

For both CAFs, the magnitudes of the zone of interest are presented in Table 3 for comparison: the mean level of the first 30 m (3 range bins), zone which will be referred to as "zero-delay wall"; the response of the target; the mean of the noise floor excluding the zero-delay wall; the mean plus one standard deviation of the noise floor excluding the zero-delay wall.

The response of the target is situated inside a delay-range bin corresponding to the expected position based on the measurement geometry; while the response is well above the noise floor, a residual zero delay wall is still present. The RCS value chosen for the simulation is chosen to be 0.11 m^2, which is consistent with that of a car at our important bistatic angle of 140° (see [19, 27]). The speed is adjusted to occupy the same Doppler cell as the real target; the propagation channel for the static paths is one measured during the campaign and chosen at random, whereas the LTE symbols are generated. Additional variation of the static channel are simulated using the same statistics as those measured, and CFO/SFO effects are also added to the received signal using the same parameters as those measured. In the figure below, results from measured signals are shown on the left column, whereas results from simulations are shown in the right column. Similarly to the aircraft target, a simulation of an ideal two receiver passive radar system is also conducted for comparison.

Due to our limited bandwidth of 20 MHz, our delay resolution is only corresponding to 10 m length range bins [9], which means that in our measurement campaign the target is only few cells/bins away from the zero-delay wall in the delay-Doppler plane. That wall is due to leftover imperfections in the received signal post-process, see next section for comparison with an ideal system. Nonetheless, the target response is well above the floor level and more importantly in-line with what the simulation predicts.

For comparison with the standard system architecture and radar process. An additional simulation has been done where, using the same dataset and parameters, but with a measured reference signal. CFO/SFO/Power variations of the transmitted signal have been set to zero, in order to simulate an ideal case where both the reference and surveillance signal would be affected the same way by these defects. Though the reference signal is affected by the exact same static propagation channel of the surveillance signal and an AWGN of the same relative level to the surveillance signal has been added. On Figure 12, a comparison of the previously presented single receiver simulation and said classical system is presented. The CAF is

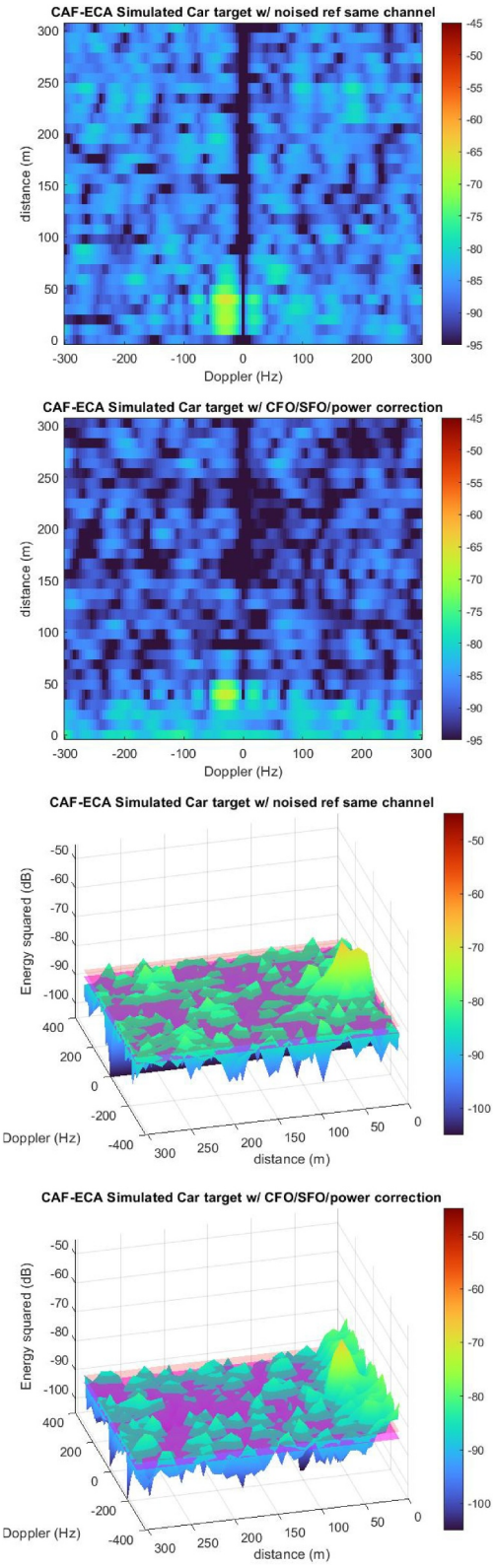

FIGURE 12 2D and 3D representation of the cross ambiguity function (CAF) for a car target, using simulation, for a standard ideal two receiver passive radar (first and third) and the proposed single receiver passive radar (second and fourth).

TABLE 4 Car target: Power levels in the delay-Doppler plane for standard/proposed system.

Adjusted ECA-C	2Rx system	1Rx system
Target response	−65.95 dB	−67.11 dB
Floor mean level	−85.61 dB	−89.34 dB
Floor mean + std level	−83.35 dB	−86.88 dB
Wall mean level	−84.87 dB	−81.55 dB
Target - (floor mean + std level)	17.40 dB	19.77 dB

represented in 2D (first pair of images) then 3D (second pair), for each of those pair, the topmost image corresponds to our single receiver system and the subsequent one corresponds to a the classical system, then Table 4 compiles the different levels of the zone of interest:

The standard system scenario represents an ideal case for such a system, and as expected, the absence of defects leads to the disappearance of the zero-delay wall. However, due to the measured nature of the reference signal and its noise therein, the overall level of the noise floor is higher while the response of the target stays comparable, when compared to our signal reconstruction system. Overall, our proposed system yields better performance for target detection outside immediate range.

4.2 | Detection of small aircraft

Fortunately, we had the opportunity to observe a small private aeroplane directly above us. We assume it was detected by our radar, as several factors support this hypothesis. First, as a word of caution, this aeroplane was not operated by us, therefore we do not have his trajectory, we also assume his destination and that it was landing given the proximity of the landing lane of a nearby airport (4 km). There are multiple elements that lead us to this assumption. No car, bike, truck or train were visibly present during the acquisition. The low Doppler of the response is coherent with the direction of the nearby airport which is close to parallel with our transmitter-receiver axis. The plane was captured from below where its RCS should be the highest. According to the operators the angular size of the target was equivalent to a fist with the arm extended which correspond to a distance of approximately 50 m, the corresponding delay would then also be around 50 m.

For this small propeller-driven aircraft target, only 5 frames (50 ms, $M = 700$) of acquisition are processed. The same processes of coarse time synchronisation, C-RS reconstruction, C-RS extraction, phase correction, ZF-Channel estimation and correction is done as before. Figure 6 shows the variations over the duration of the acquisition of the estimated ZF-Channel, for port 1 and 2, respectively. The variation and amplitude of the mean and standard deviation of the channel are extremely

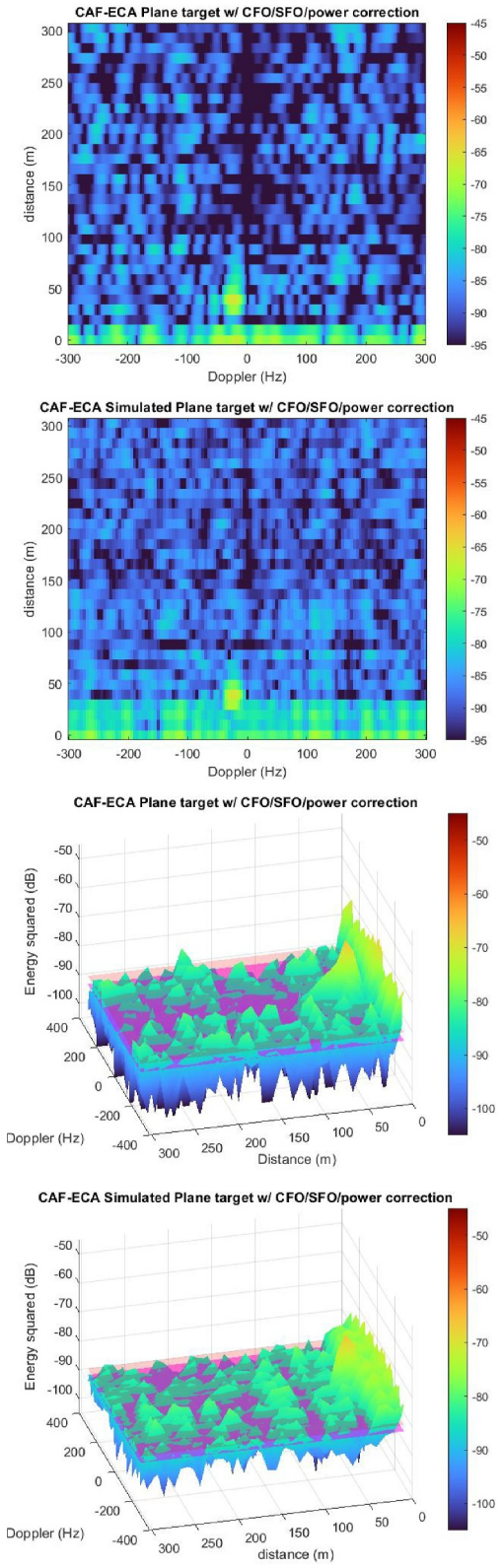

FIGURE 13 3D representation of the cross ambiguity function (CAF) post adjusted ECA-C, for an aircraft target, using both real measurement (first and third) and simulation (second and fourth).

similar as the previous acquisition; however, the "seesaw pattern" is more pronounced, highlighting the unpredictability of the variations of emitted C-RS.

TABLE 5 Aircraft target: Power levels in the delay-Doppler plane for adjusted ECA-C.

Adjusted ECA-C	Real	Simulations
Target response	−65.88 dB	−65.92 dB
Floor mean level	−88.27 dB	−87.72 dB
Floor mean + std level	−85.34 dB	−85.38 dB
Wall mean level	−76.64 dB	−76.44 dB
Target - (floor mean + std level)	19.46 dB	19.46 dB

As was done in the previous case, the result of the CAF calculated post adjusted ECA-C will be compared to a simulation. The same value of the RCS for the target is used (0.11 m^2). The speed is also adjusted to occupy the same Doppler cell as the real target; the propagation channel for the static paths and its variation are those measured, as are the CFO/SFO effects. On Figure 13, results from measured signals are shown on the first and third graphics whereas results from simulations are shown in the second and fourth graphics.

The magnitudes of the four zone of interest are compiled for comparison in Table 5.

The response of the target is well above the noise floor; however, a residual zero delay wall remains present. The RCS value chosen for the simulation is also in line with the measured response. As was done for the car target, a simulation of an ideal two receiver passive radar system is also done for comparison. The results are shown in Figure 14 and Table 6.

The simulated two receiver process does not produce a zero-delay wall in the delay-Doppler space, whereas the single receiver one does. However the noise floor level of the two receiver process is elevated more than the target response is when comparing with the single receiver process, leading to a lesser power margin between the target response and the noise floor. Overall, while the single receiver process is still partially blinded in the near zero-delay surveillance area, it is again expected to yield better results everywhere else.

5 | CONCLUSION

This paper presents a successful implementation of OFDM passive radar techniques for target detection exploiting LTE opportune signals and using a single receiver thanks to signal reconstruction techniques. The nature of the channel reference signal make this method's viability independent of telecom traffic state, thus reliable at any time. Experiment showing detection of targets were shown and confirmed the predicted performance of the system. Furthermore, said performances are shown to be superior to those of a standard architecture. However, the system demonstrated in this article is incomplete as it achieves construction of the delay-Doppler plane only. While formal detection could easily be achieved using constant false alarm rate methods, which is ubiquitous in passive radar, target localisation will require additional spatial information. Classically this is done with beam-forming techniques

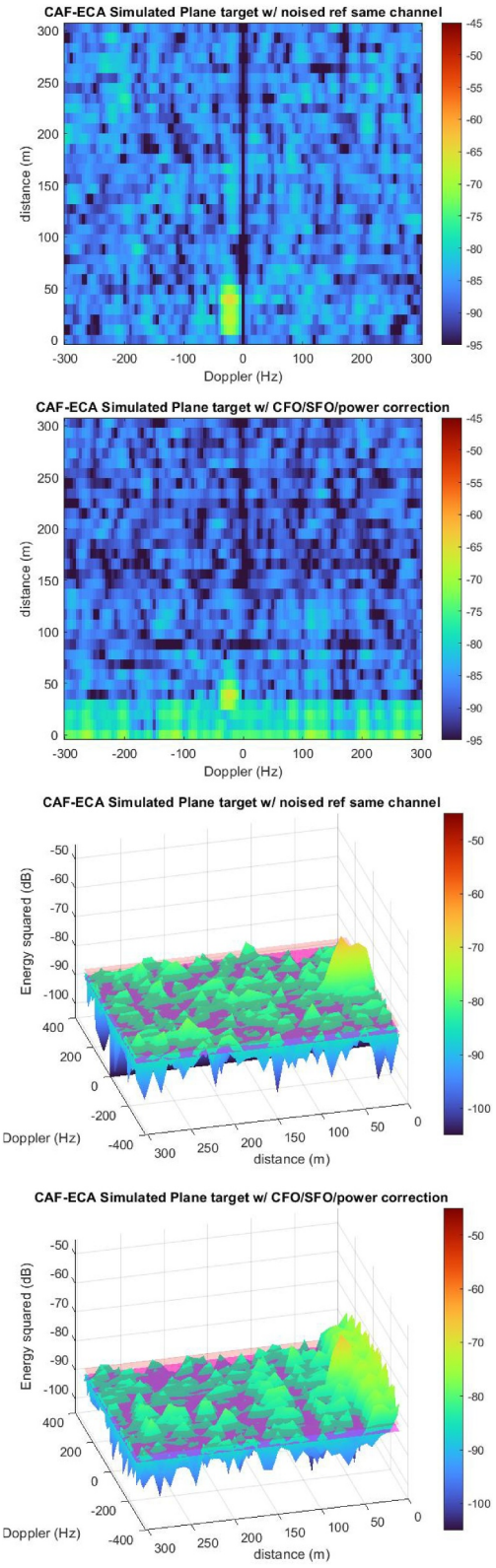

FIGURE 14 2D and 3D representation of the cross ambiguity function (CAF) for an aircraft target, using simulation, for a standard ideal two receiver passive radar (first and third) and the proposed single receiver passive radar (second and fourth).

TABLE 6 Aircraft target: Power levels in the delay-Doppler plane for standard/proposed system.

Adjusted ECA-C	2Rx system	1Rx system
Target response	−64.79 dB	−65.92 dB
Floor mean level	−85.34 dB	−87.72 dB
Floor mean + std level	−83.07 dB	−85.38 dB
Wall mean level	−85.17 dB	−76.44 dB
Target - (floor mean + std level) (dB)	18.28 dB	19.46 dB

exploiting spatial diversity at the receiver; if the single receiver aspect was to be pursued, multiple detections with regards to different BS could be made with this single receiver, allowing triangulation to enable localisation. As is commonly discussed among similar works, real-time implementation of the proposed method is a realistic prospect thanks to performance of the OFDM algorithms in the frequency domain.

AUTHOR CONTRIBUTIONS

Lionel de Guenin: Formal Analysis; methodology; writing – Original Draft preparation. **Patrick Rosson**: Investigation; resources; validation; supervision; writing – Review and Editing. **Nicolas Petrochilos**: Methodology; supervision; writing – Review and Editing. **Eric Moreau**: Supervision; project Administration; writing – Review and Editing.

FINANCIAL DISCLOSURE

None reported.

CONFLICT OF INTEREST STATEMENT

The authors declare no potential conflict of interests.

DATA AVAILABILITY STATEMENT

The data that support the findings of this study are available from the corresponding author upon reasonable request.

ORCID

Lionel de Guenin https://orcid.org/0009-0007-2572-6173

REFERENCES

1. Berger, C.R., et al.: Signal processing for passive radar using OFDM waveforms. IEEE Journal of Selected Topics in Signal Processing 4(1), 226–238 (2010). https://doi.org/10.1109/JSTSP.2009.2038977
2. Gassier, G., et al.: A unifying approach for disturbance cancellation and target detection in passive radar using OFDM. IEEE Trans. Signal Process. 64(22), 5959–5971 (2016). https://doi.org/10.1109/TSP.2016.2600511
3. Pecoraro, G., et al.: CSI-based fingerprinting for indoor localization using LTE Signals. In: EURASIP Journal on Advances in Signal Processing (2018). https://doi.org/10.1186/s13634-018-0563-7
4. Raout, J.: Sea target detection using passive DVB-T based radar. In: 2008 International Conference on Radar, pp. 695–700. Adelaide, SA, Australia (2008). https://doi.org/10.1109/RADAR.2008.4654010
5. Vorobev, E.N.: Helicopter recognition in DVB-T2 passive bistatic radar. In: 2018 IEEE Conference of Russian Young Researchers in Electrical and Electronic Engineering (EIConRus), pp. 1171–1173. Moscow and St.

Petersburg, Russia (2018). https://doi.org/10.1109/EIConRus.2018.8317299
6. Bartoletti, S., Conti, A., Win, M.Z.: Passive radar via LTE signals of opportunity. In: 2014 IEEE International Conference on Communications Workshops (ICC), pp. 181–185. Sydney, NSW, Australia (2014). https://doi.org/10.1109/ICCW.2014.6881193
7. Rai, P.K., et al.: LTE-based passive radars and applications: a review. Int. J. Rem. Sens. 42(19), 7489–7518 (2021). https://doi.org/10.1080/01431161.2021.1959669
8. Evers, A., Jackson, J.A.: Analysis of an LTE waveform for radar applications. In: 2014 IEEE Radar Conference, pp. 0200–0205. Cincinnati, OH, USA (2014). https://doi.org/10.1109/RADAR.2014.6875584
9. Wang, J., Zhang, B., Lei, P.: Ambiguity function analysis for OFDM radar signals. In: 2016 CIE International Conference on Radar (RADAR), pp. 1–5. Guangzhou, China (2016). https://doi.org/10.1109/RADAR.2016.8059592
10. Maksymiuk, R., et al.: Rényi entropy-based adaptive integration method for 5G-based passive radar drone detection. Rem. Sens. 14(23), 6146 (2016). https://doi.org/10.3390/rs14236146
11. O'Hagan, D.W., et al.: Signal reconstruction as an effective means of detecting targets in a DAB-based PBR. In: 11-th INTERNATIONAL RADAR SYMPOSIUM, pp. 1–4. Vilnius, Lithuania (2010)
12. Zemmari, R.: Reference signal extraction for GSM passive coherent location. In: 11-th INTERNATIONAL RADAR SYMPOSIUM, pp. 1–4. Vilnius, Lithuania (2010)
13. Maslikowski, L., et al.: Passive bistatic SAR imaging — challenges and limitations. IEEE Aero. Electron. Syst. Mag. 29(7), 23–29 (2014). https://doi.org/10.1109/MAES.2014.130141
14. Baczyk, M.K., Malanowski, M.: Decoding and reconstruction of reference DVB-T signal in passive radar systems. In: 11-th INTERNATIONAL RADAR SYMPOSIUM, pp. 1–4. Vilnius, Lithuania (2010)
15. Berthillot, C., et al.: BEM reference signal estimation for an airborne passive radar antenna array. IEEE Trans. Aero. Electron. Syst. 53(6), 1–2845 (2017). https://doi.org/10.1109/TAES.2017.2716458
16. Cristallini, D., Hagan, D.: Passive Radars on Moving Platforms. Institution of Engineering and Technology (2023)
17. Di Seglio, M., et al.: Comparing reference-free WiFi radar sensing approaches for monitoring people and drones. IET Radar, Sonar Navig. 18, 1–18 (2023). https://doi.org/10.1049/rsn2.12506
18. LTE, Evolved Universal Terrestrial Radio Access (E-UTRA): Physical channels and modulation3GPP TS 36.211 version 12.9.0 Release 12 118 ETSI TS 136 211 V12.9.0 (2017)
19. Blázquez-García, R., Casamayón-Antón, J., Burgos-García, M.: LTE-R based passive multistatic radar for high-speed railway network surveillance. In: 2018 15th European Radar Conference (EuRAD), pp. 6–9 (2018). Madrid, Spain. https://doi.org/10.23919/EuRAD.2018.8546516
20. Youssef, N., Jean-François, H., Matthieu, C.: On the influence of carrier frequency offset and sampling frequency offset in MIMO-OFDM systems for future digital TV. 2008 3rd International Symposium on Wireless Pervasive Computing, 93–96 (2008). https://doi.org/10.1109/iswpc.2008.4556173
21. Yong-An, J., Sung-Jin, K., Young-Hwan, Y.: A robust SFO estimation scheme for OFDM-based DRM with non-symmetric distributed pilots. Wireless Pers. Commun. 88(4), 749–760 (2016). https://doi.org/10.1007/s11277-016-3199-7
22. Kamal Khairiee bin Yahya, N.M., et al.: Drone's radar cross section computation for various reflected angles using LTE frequency. In: 2019 IEEE Asia-Pacific Conference on Applied Electromagnetics (APACE), pp. 1–4 (2019). https://doi.org/10.1109/APACE47377.2019.9020826
23. SRM User Group: Distributed by: Air-Met Scientific Pty Ltd. Work with Confidence. Air-Met Sales/Service. P: 1800 000 744. F: 1800 000 774 (2016)
24. Colone, F., et al.: A multistage processing algorithm for disturbance removal and target detection in passive bistatic radar. IEEE Trans. Aero. Electron. Syst. 45(2), 698–722 (2009). https://doi.org/10.1109/TAES.2009.5089551
25. Schwark, C., Cristallini, D.: Advanced multipath clutter cancellation in OFDM-based passive radar systems. In: 2016 IEEE Radar Conference (RadarConf), pp. 1–4. P (2016). hiladelphia, PA, USA. https://doi.org/10.1109/RADAR.2016.7485166
26. Technical notice fo the oscar 20, 4G yagi antenna; https://www.farnell.com/datasheets/2213163.pdf
27. Noor Hafizah, A.A., et al.: RCS analysis on different targets and bistatic angles using LTE frequency. In: 2015 16th International Radar Symposium (IRS), pp. 658–663 (2015). Dresden, Germany. https://doi.org/10.1109/IRS.2015.7226397

How to cite this article: de Guenin, L., et al.: Single receiver Long-Term Evolution passive radar system using signal reconstruction for moving target detection. IET Radar Sonar Navig. 18(12), 2400–2413 (2024). https://doi.org/10.1049/rsn2.12662